AIMS Materials Science, 10(1): 86–111.
DOI: 10.3934/matersci.2023006
Received: 03 October 2022
Revised: 05 December 2022
Accepted: 21 December 2022
Published: 12 January 2023

http://www.aimspress.com/journal/Materials

Research article

Modeling the flexural strength of steel fibre reinforced concrete

Abdul Saboor Karzad[1,*], Moussa Leblouba[2], Zaid A. Al-Sadoon[2], Mohamed Maalej[2] and Salah Altoubat[2]

[1] Department of Civil Engineering, University of Ottawa, Ottawa, Ontario, Canada
[2] Department of Civil and Environmental Engineering, University of Sharjah, Sharjah, UAE

*** Correspondence:** Email: akarzad@uottawa.ca.

Abstract: Industrial applications of fibre-reinforced concrete (FRC) in structures require extensive experimental and analytical investigations of the FRC material properties. For design purposes and applications involving the flexural loading of the member, it is essential to have a predictive model for the flexural strength of the FRC material. In the present paper, a fracture mechanics approach based on Bridged Crack Model (BCM) is used to predict the flexural strength of steel fibre-reinforced concrete (SFRC) beams. The model assumes a quadratic tension-softening relationship (σ–δ) governing the bridging action of the steel fibres and a linear profile of the propagating crack. The proposed tension-softening relationship is considered valid for a wide range of fibre-reinforced concrete materials based on the knowledge of either the material micromechanical parameters (such as fibre volume fraction, fibre/matrix bond strength, fibre length, and fibre tensile strength) or an actual experimentally-measured σ–δ relationship. The flexural strength model thus obtained allows the prediction of the flexural strength of SFRC and study the variation of the latter as a function of the micromechanical parameters. An experimental program involving the flexural testing of 13 SFRC prism series was carried out to verify the prediction of the proposed model. The SFRC mixes incorporated two types of steel fibres (straight-end and hooked-end), four different concrete compressive strengths (40, 50, 60, and 70 MPa), three different fibre volume fractions (1, 1.5, and 2%), and three specimen depths (100, 150, and 200 mm). The experimental results were compared to the predictions of the proposed flexural strength model, and a reasonable agreement between the two has been observed. The model provided a useful physical explanation for the observed variation of flexural strength as a function of the test variables investigated in this study.

Keywords: concrete; fibre-reinforced materials; fracture mechanics; flexural strength; beam

Nomenclature

a, a_i	Crack length (of the major crack), the initial value of crack length (mm)
b	Width of prism specimen (mm)
c	Normalized value of x ($=x/a$)
d	Depth of prism specimen (mm)
d_f	Fibre diameter (mm)
E_c	Modulus of elasticity of concrete (MPa)
E_f	Modulus of elasticity of fibre (MPa)
f	Snubbing friction coefficient that affects the parameters T_B, k, and p of the tension softening relationship as described in [14]
$f(s)$	Calibration function for computing crack-mouth-opening displacement w_σ
f_3	Calibration function for stress intensity factor K_{IM}
g, g_i	Calibration functions for Stress intensity factor $K_{I\sigma}$
f_{cu}	Concrete cube compressive strength (MPa)
I	Integration term in equation 8
k, p	Parameters that describe the shape of the tension-softening curve
K_I	Stress intensity factor (MPa $\sqrt{m}^{1/2}$)
$K_{I\sigma}$	Stress intensity factor due to closing traction of the bridging fibres (MPa $\sqrt{m}^{1/2}$)
K_{IC}	Critical intensity factor (MPa $\sqrt{m}^{1/2}$)
K_{IM}	Stress intensity due to bending moment M (MPa $\sqrt{m}^{1/2}$)
L	Clearspan of prism specimen (mm)
L_f	Fibre length (mm)
M	Bending moment in the central position (constant moment region) of the prism specimen (kN $\sqrt{m}$)
P_u	Maximum load measured at which the prism specimen fails (kN)
r, r_i	Normalized value of a, a_i ($=a/d$, ai/d)
t	New term introduced in the change of variable x ($x=asint$)
T_b	Post-cracking tensile strength of SFRC (MPa)
s	Normalized value of x (=x/d)
u	Normalized crack-mouth-opening displacement ($=w/w_c$)
V	Calibration function for computing crack-mouth-opening displacement w_M
V_f	Fibre volume fraction (%)
w	Crack-mouth-opening displacement (mm)
w_σ	Crack-mouth-opening displacement due to closing traction of bridging fibres (mm)
w_c	Crack-mouth-opening displacement at which the fibre bridging stress becomes zero (mm)
w_M	Crack-mouth-opening displacement due to bending moment M (mm)
x	Distance along the length of the major crack, measured from the beam tensile face, at which the crack opening displacement or fibre bridging stress is computed
Δ	Midspan deflection (mm)
δ	Major crack opening displacement at a distance x from the beam tensile face (mm)
σ	Fibre bridging stress in the stress vs crack opening (σ–δ) displacement relationship
ε	Strain in the tensile stress-strain (σ–ε) relationship used to model the bridging effect of the fibre
σ_f	Flexural stress at the extreme tensile face of the beam ($6M/bd^2$) (MPa)

σ_I Fibre bridging stress at a distance *x* from the beam tensile face (MPa)
τ Fibre / Matrix interfacial bond strength (MPa)

1. Introduction

1.1. Background

Fibre-reinforced concrete (FRC) is a composite material made of conventional concrete and discrete short fibres made of different materials and geometries. FRC is known for its enhanced post-cracking behaviour and energy absorption compared to OPC concrete. The use of FRC in the construction industry has been increasing over the past three decades, and the most commonly used is Steel Fibre Reinforced Concrete (SFRC). Field applications of FRC included airport runways, tunnel linings, bridge structures, and protective structures, to name a few. Using short, randomly distributed fibres in concrete has been shown to increase the flexural strength and toughness of the material and contribute to better crack control. Various enhancements in such properties were achieved depending on the properties of the concrete matrix, fibre and fibre/matrix interface. In a flexural-loaded FRC beam, such enhancements are mainly influenced by the fibre-bridging stress distribution acting across the first crack that develops on the tensile face of the beam. The latter is part of what is referred to in the literature as the Fracture Process Zone (FPZ) [1,2].

In concrete, Hillerborg et al. [3] assumed that the FPZ starts to develop at locations where the maximum principal stress reaches the material's tensile strength. When a crack forms, the stress at the crack mouth is assumed not to fall to zero immediately but instead starts to decrease with increasing crack opening according to the tension-softening relationship. The stress is assumed to fall to zero only when the crack-mouth-opening reaches a critical value w_c. These assumptions are part of Hillerborg's fictitious crack model (FCM) [4] that was used to relate the flexural strength of concrete to its uniaxial tensile strength. Because of the FPZ, the flexural strength of concrete was greater than its tensile strength. The size of the FPZ relative to the specimen depth has been recognized as an important factor governing the flexural strength-to-tensile strength ratio, and this has been referred to in the literature as size effect [5], where the flexural strength of concrete was found to decrease with increasing specimen depth.

After Hillerborg's FCM model (also found in the literature under the name of the cohesive crack model), researchers developed other models based on modified linear-elastic fracture mechanics (LEFM) approaches. Among such models is the bridged crack model (BCM) initially developed by Carpinteri [6,7] for concrete reinforced by steel bars. In the BCM, crack propagation in concrete was assumed to be governed by a *stress intensity factor* (K_I) criterion instead of a strength-based criterion (used in the cohesive crack model). Ahead of the crack tip, the stress distribution was assumed to be directly related to the magnitude of the stress intensity factor, which depends on the specimen configuration, the applied load, and the crack-closing force of the steel reinforcement (acting across the crack faces). Other such models included the size-effect model [8], the crack band model [9], the two-parameter fracture model [10], and the double-K fracture model [11–13].

In an attempt to develop a predictive model for the flexural strength of FRC, Maalej and Li [14] used the FCM to relate the flexural strength to the material tension softening $(\sigma - \delta)$ properties and

specimen geometry. An analytical expression for the $(\sigma - \delta)$ relationship has previously been developed by Maalej et al. [15] for FRC as a function of the matrix, fibre, and matrix/fibre interface properties taking into account the effect of both fibre pull-out and fibre rupture. In their flexural strength model, Maalej and Li [14] assumed that a major crack would initially form at the tensile face of the beam and then starts to propagate once the tensile stress (at the tensile face of the beam) reaches the uniaxial tensile strength of the material. As the crack propagates, a FPZ starts to develop where the reinforcing fibres will bridge the faces of the crack, thereby transferring bridging stresses with magnitudes that depend on the fibre and fibre/matrix interface properties and the crack width. Similar to concrete, the model had shown that the flexural strength is reached when the FPZ is partially developed.

Zhang and Li [16] used a fracture-mechanics approach based on the BCM [6,7] to simulate the crack propagation in FRC, where the crack-closing action of the steel reinforcement in the BCM was replaced by the distributed bridging action of the reinforcing short fibres acting across the crack faces in the FRC cracked section. As the crack propagates, the FPZ increases in size and contributes to lowering the effective stress intensity factor, resulting in increasing the magnitude of the applied load required for further crack propagation. The model contributed towards a better understanding of crack propagation in FRC and how it is affected by the action of fibre reinforcement in the composite.

More recently, an extension of the BCM (Updated Bridged Crack Model) has been proposed to model crack propagation in concrete with either or both steel bars and short fibre reinforcement [17–21]. The model was used to predict the full flexural response of FRC beams and hybrid reinforced concrete (HRC) beams (beams that incorporate both regular steel reinforcement and short fibres), taking into consideration the bridging action of the short fibres in addition to the yielding of the steel bars in the case of HRC beams. For FRC beams, the model could predict the different flexural response stages (elastic, post-cracking, pull-out) and capture the scale effect in the structural behaviour of such beams.

In the present study, the BCM is used together with a specific tension-softening relationship (σ–δ) governing the bridging action of the steel fibres and a linear profile of the propagating crack to predict the flexural strength of SFRC. The proposed tension-softening relationship is assumed to be valid for a wide range of fibre-reinforced concrete materials based on the knowledge of either the material micromechanical parameters (such as fibre volume fraction, fibre/matrix bond strength, fibre length, and fibre tensile strength) or an actual experimentally-measured σ–δ relationship. The model thus obtained allows the prediction of the flexural strength of SFRC and the study of the variation of the latter as a function of the micromechanical parameters. As such, the model contributes towards a better understanding of the physical mechanisms governing the flexural strength of SFRC.

In addition to the above modeling component, the present study includes an experimental program involving 13 SFRC prism series that were subjected to 4-point flexural testing. The test variables in the experimental program included the specimen depth (100, 150, and 200 mm), the volume fraction of steel fibres in the mix (1%, 1.5% and 2%), the fibre type (hooked-end and straight-end steel fibres) and the concrete cube compressive strengths (40, 50, 60, and 70 MPa). A comparison of the model-predicted and experimentally-measured flexural strengths was made to evaluate the validity of the proposed flexural strength model.

1.2. Summary of related studies

In addition to the studies highlighted in the previous section, other relevant studies presented analytical procedures for predicting the flexural strength of FRC and the moment capacity of reinforced concrete elements that incorporate short fibre reinforcement. These studies are focused on measuring fracture-related properties from flexural test data using inverse analysis approaches, and applying non-destructive techniques such as Digital Image Correlation (DIC) and Acoustic Emission (AE) to monitor the fracture process in concrete and FRC. This section provides a summary of some of these studies.

Lok and Xiao [22] presented an analytical model based on the tensile stress-strain (σ–ε) relationship to predict the moment-curvature behaviour of SFRC. A bilinear relationship modeled the softening branch in the stress-strain diagram. The role of fibre volume fraction and interfacial properties of fibre-matrix in affecting the behaviour of SFRC in flexure was considered. The flexural strength prediction of their model was compared to experimental data obtained from tests conducted on beams and slabs. The model predictions were found to agree with the data from experimental test results.

Meng et al. [23] proposed a four-linear model for the stress-strain (σ–ε) relationship in tension and a triangular stress block for compression to analyze and predict the load-deflection behaviour of SFRC prisms in flexure. The four-linear proposed model consists of four stages: pre-cracked, at the cracking moment, crack propagation, and failure. The authors included an experimental phase to verify their proposed model and determine the residual strength of corresponding stages. In the experimental phase, SFRC prisms of 150 × 150 × 550 mm with two dosage rates of fibres (i.e., 30 kg/m^3 and 40 kg/m^3) were cast and tested as per the EN 14651 test standard. The results indicated a fair prediction of their proposed model against the experimental data.

More recently, Zheng et al. [24] studied the Flexural behaviour of FRP grid-reinforced ultra-high-performance concrete (UHPC) composite plates incorporating different fibres. In their study, they proposed a model for the FRP grid-reinforced UHPC plates' flexural capacity that considers the contribution of the steel/polyethylene (PE) fibre in the UHPC. An equivalent stress distribution was used to represent the tensile stress of steel/PE fibre-reinforced UHPC in the tensile zone after cracking (assumed equal to the UHPC initial cracking strength). The results showed a reasonable agreement between predicted and measured moment capacities of FRP grid-reinforced UHPC.

In the literature, studies focused on measuring the fracture parameters of the concrete material from flexural test data using an inverse analysis approach. In this approach, concrete's cracking tensile strength is considered a starting point of the σ–δ curve, providing a criterion to check if crack propagation has started. One such example is the work of Soetens and Matthys [25], where two variants of a model were proposed (i.e., a tri-linear post-cracking behaviour model and an analytical model). The trilinear Mode-I constitutive model was derived based on the inverse analysis, while the analytical model has based on the single fibre pull-out simulated response. Mode-I constitutive law was estimated using an inverse analysis approach and a tri-linear crack opening law adaptation in modeling the first variant. The second variant was developed to estimate the crack bridging characteristic of SFRC in the uni-axial direction resulting in Mode-I constitutive law. The experimental program of their study consisted of three- and four-point bending tests on 42 SFRC

prisms with dimensions of 150 × 150 × 600 mm to obtain residual flexural parameters. Their findings suggested a good match between the two variants of their proposed model and a good correlation with the experimental results.

Another example is the research presented by Zhang et al. [26] based on the inverse analysis approach. The method is proposed to determine the fracture parameters of concrete, such as cracking and tensile strength, stress-crack relationship, and fracture energy. The method, which relies on the FCM, is developed from simple three-point bending test results and can be used to investigate the effect of aggregate size and concrete compressive strength on fracture-related parameters. The experimental program consisted of deformation-controlled three-point bending tests of 400 × 100 × 100 prisms. The prisms were cast of concrete with normal and high compressive strength (i.e., 40 MPa and 80 MPa) that incorporated four different aggregate sizes. The results revealed that the size of coarse aggregate and the strength of concrete have a noticeable effect on the stress-crack (σ–w) relationship of normal-strength concrete. However, this effect is not evident in the stress-crack relationship of high-strength concrete. Moreover, the aggregate size had a similar effect on other fracture parameters, such as characteristic length and fracture energy for both normal and high-strength concrete.

Da Silva et al. [27] presented an integrated approach incorporating a multiscale model to simulate and predict the flexural behaviour of SFRC elements. In the proposed model, the pull-out resistance of fibres was evaluated at the microstructural level by modeling the fibre as a one-dimensional continuum considering the fibre geometry, distribution, and orientation. Further, a cohesive-like constitutive law was considered to account for the concrete in compression and the interface between fibre and the concrete to simulate the interaction between the fibres and the surrounding concrete. The three main and possible local failures, such as fibre rupture and debonding, matrix damage, and matrix spalling, were incorporated in the proposed micromechanical approach. The authors evaluated the validity of this approach using data collected from experimental studies on the pull-out response of a single fibre. The verification of the model proved that the proposed approach, which is based on inverse analysis, can determine the stress vs. crack width relationship of FRC material.

A new method based on a non-destructive approach called Digital Image Correlation (DIC) along with Acoustic Emission (AE) is emerging in the experimental mechanics of materials as a potential method to monitor the fracture process of quasi-brittle materials such as concrete [28,29]. For instance, Chen et al. [30] adopted DIC and AE to identify the fracture damage characteristics of fibre-reinforced cement-based composites. Their study evaluated the fracture behaviour of ultra-high performance fibre-reinforced cement-based composites (UHPFRCC). Three-point loading tests were carried out on UHPFRCC prisms with a fibre dosage of 1% and 2%, while the fracture process was monitored using DIC and AE techniques. The AE technique was used to identify the failure of the matrix and debonding of matrix/fiber through two algorithms, namely, a supervised KNN method and an unsupervised k-means clustering method. The results were verified by the DIC method, which was used to analyze the mechanism of fracture damage. The study concluded with a model for identifying the behaviour of UHPFRCC in terms of matrix/fibre debonding and matrix failure based on a supervised KNN algorithm. He et al. [31] have also adopted the DIC technique to study the fracture behaviour of hybrid steel fibre-reinforced concrete (HSFRC), including quantitatively

describing and analyzing the Fracture Process Zone (FPZ) and damage characteristics. Notched prisms with 0% to 2% fiber volume fraction were tested under a three-point loading scheme. The test results indicated that the fracture process develops in four phases: propagation of microcrack, formation of fracture, the rapid expansion of fracture, and unstable post-peak. They found that adding fibres affects the development and growth of FPZ length; however, the effect of the hybrid combination on FPZ growth is negligible. The increase of fibre volume fraction from 0 to 2% resulted in an increase in critical FPZ length from 21.6 to 79.1 mm.

2. Materials and methods

2.1. Modeling of the flexural strength

A fracture mechanics model for predicting the flexural strength of fibre-reinforced concrete is presented in this section. The model follows the bridged crack model (BCM) approach by Carpinteri [6,7] but assumes a quadratic tension-softening relationship governing the bridging action of the steel fibres and a linear profile of the propagating crack. This model will later be used to predict the flexural strength of SFRC prim specimens from a companion experimental program.

2.1.1. Assumed tension-softening relationship

Consider a rectangle beam made with steel fibre-reinforced concrete having a span L, depth d, and width b. The beam is loaded in a four-point bending configuration resulting in a constant bending moment in the central portion of the beam.

Figure 1 shows a cracked section of a beam subjected to a bending moment M. The crack length and crack-mouth-opening are assumed equal to a and w, respectively. Within the FPZ, the bridging stress $\sigma_1(x)$ is assumed to decrease as a function of crack width δ according to the tension-softening relationship [14]:

$$\sigma_1(x) = T_b\left[1 - 2k\left(\frac{\delta}{w_c}\right) + p\left(\frac{\delta}{w_c}\right)^2\right] \tag{1}$$

This equation is assumed to be valid for a wide range of fibre-reinforced concrete materials with given material micromechanical parameters or experimentally-measured tension-softening relationship (corresponding to specific T_b, w_c, k, and p values). In this equation, T_b represents the post-cracking strength of the composite, w_c represents the Crack Opening Displacement (COD) at which the bridging stress becomes zero, and k and p represent the initial slope and curvature of the tension-softening curve, respectively. With an assumption of a linear crack profile within the FPZ, the crack width δ at any point x is assumed to vary with crack-mouth-opening w according to the following equation:

$$\delta = w\left(1 - \frac{x}{a}\right) \tag{2}$$

Therefore, the distribution of the normal stresses within the FPZ is given by the following equation:

$$\sigma_1(x) = T_b\left[1 - 2ku\left(1 - \frac{x}{a}\right) + pu^2\left(1 - \frac{x}{a}\right)^2\right] \tag{3}$$

where $u = w/w_c$.

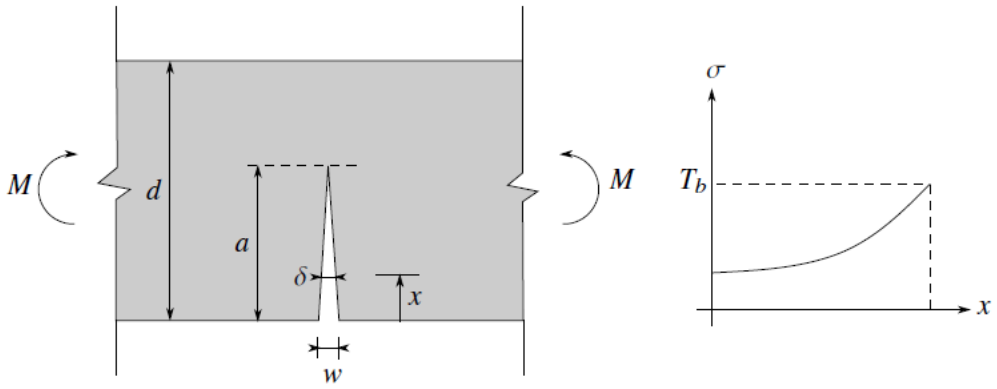

Figure 1. Tension softening curve across the fictitious crack section.

2.1.2. Stress intensity factor

Consider the central portion of the beam, which is subjected to a constant moment M resulting from the four-point flexural loading of the beam specimen. It is assumed that during the beam's loading, a (fictitious) crack of length a will form on the beam's tensile face. Following the BCM approach, the stress intensity factor at the crack's tip is assumed to consist of two parts. The first part (positive) is caused by the bending moment M, and the second part (negative) is caused by the closing traction acting on the fictitious crack due to the bridging action of the fibres. Physically, the first term will contribute towards increasing the COD, while the second term will contribute towards reducing it. Once the total stress intensity factor K_I at the tip of a crack reaches the material fracture toughness, K_{IC}, the crack will start to propagate.

(a) Stress intensity factor due to the applied moment M

For a notched beam specimen subjected to a bending moment M, the stress intensity factor is given by [32]:

$$K_{IM} = \sigma_f\sqrt{\pi a}\ f_3\left(\frac{a}{d}\right) \tag{4}$$

where $\sigma_f = 6M/bd^2$ is the stress at the extreme tensile surface of the beam and $f_3\left(\frac{a}{d}\right)$ is given by:

$$f_3\left(\frac{a}{d}\right) = \sqrt{\frac{2d}{\pi a}\tan\left(\frac{\pi a}{2d}\right)}\,\frac{0.923 + 0.199\left(1 - \sin\frac{\pi a}{2d}\right)^4}{\cos\frac{\pi a}{2d}} \tag{5}$$

(b) Stress intensity factor due to fibre closing traction

Using the fibre stress distribution $\sigma_1(x)$ acting across the crack (see Figure 1), and the stress intensity factor equation given by Tada et al. [32] for a single-edge notched specimen subjected to a concentrated force P applied at a distance x from the mouth of the crack, one can write an expression for the stress intensity factor equation $K_{I\sigma}$ due to the closing traction of the bridging fibres given by the fibre stress distribution $\sigma_1(x)$ as follows:

$$K_{I\sigma} = \int_{a_i}^{a} \frac{2\sigma_1(x)\ g\left(\frac{x}{a},\frac{a}{d}\right)}{\sqrt{\pi a}\left(1-\frac{a}{d}\right)^{1.5}\left[1-\left(\frac{x}{a}\right)^2\right]^{0.5}}\,dx \tag{6}$$

where a_i is an assumed initial flaw size and a is the total length of the crack. The function $g(c,r)$ is a polynomial given by the following equation:

$$\begin{aligned} g(c,r) &= g_1(r) + g_2(r)c + g_3(r)c^2 + g_4(r)c^3 \\ g_1(r) &= 0.46 + 3.06r + 0.84(1-r)^5 + 0.66r^2(1-r)^2 \\ g_2(r) &= -3.52r^2 \\ g_3(r) &= +6.17 - 28.22r + 34.54r^2 - 14.39r^3 - (1-r)^{1.5} - 5.88(1-r)^5 - 2.64r^2(1-r)^2 \\ g_4(r) &= -6.63 + 25.16r - 31.04r^2 + 14.41r^3 + 2(1-r)^{1.5} + 5.04(1-r)^5 + 1.98r^2(1-r)^2 \end{aligned} \tag{7}$$

where in the above equations $c = x/a$ and $r = a/d$. Using the change of variable $x = \sin t$ and the expression for the normal stresses distribution $\sigma_1(x)$ within the FPZ, the following is obtainined:

$$K_{I\sigma} = \frac{2T_b a}{\sqrt{\pi a}\left(1-\frac{a}{b}\right)^{1.5}} \int_{\arcsin\left(\frac{a_i}{a}\right)}^{\frac{\pi}{2}} [1 - 2ku(1-\sin t) + pu^2(1-\sin t)^2]\, g\left(\sin t, \frac{a}{d}\right) dt$$

or

$$K_{I\sigma} = \frac{2T_b a}{\sqrt{\pi a}\left(1-\frac{a}{b}\right)^{1.5}} I\left(u, \frac{a_i}{d}, \frac{a}{d}\right) \tag{8}$$

where the integral $I\left(u, \frac{a_i}{d}, \frac{a}{d}\right)$ can be computed analytically or numerically. Using the principle of superposition, the total stress intensity factor K_I at the tip of the crack can, therefore, be computed as follows:

$$K_{IC} = K_{IM}(\sigma_f, d, r) - K_{I\sigma}(T_b, d, u, r_i, r) \tag{9}$$

2.1.3. Crack-mouth-opening Displacement, *CMOD*

(a) *CMOD* due to closing traction

Using the equation for the stress intensity factor $K_{I\sigma}$ due to the closing traction $\sigma_1(x)$ of the bridging fibres, one can compute the $CMOD$, w_σ, due to this closing traction as follow:

$$w_\sigma = \frac{2b}{E_c}\int_{a_i}^{a} K_{I\sigma}(x)\frac{\partial K_{IF}(x)}{\partial F}dx \tag{10}$$

or

$$w_\sigma(T_b, E_c, d, u, r_i, r) = \frac{8T_b}{\pi E_c}\int_{a_i}^{a} I\left(u, \frac{a_i}{d}, \frac{x}{d}\right) f\left(\frac{x}{d}\right)\left(1-\frac{x}{d}\right)^{-1.5} dx \tag{11}$$

where

$$\begin{cases} r & = \dfrac{a}{d} \\ r_i & = \dfrac{a_i}{d} \\ f(s) & = \dfrac{0.46 + 3.06s + 0.84(1-s)^5 + 0.66s^2(1-s)^2}{(1-s)^{1.5}} \\ s & = \dfrac{x}{d} \end{cases}$$

(b) *CMOD* due to loading

For a notched beam specimen subjected to a bending moment M, the $CMOD$ is given by Tada et al. [32]:

$$w_M = \frac{4\sigma_f a}{E_c}\ V\left(\frac{a}{d}\right) \tag{12}$$

where $V\left(\frac{a}{d}\right) = 0.8 - 1.7\left(\frac{a}{d}\right) + 2.4\left(\frac{a}{d}\right)^2 + \frac{0.66}{\left(1-\frac{a}{d}\right)^2}$, and E_C is the modulus of elasticity of the SFRC material.

The actual crack-mouth-opening displacement w is then equal to the $CMOD$ due to the bending moment M minus the $CMOD$ caused by the bridging action of fibres (principle of superposition). That is:

$$w = w_M(\sigma_f, E_c, d, r) - w_\sigma(T_b, E_c, d, u, r_i, r) \tag{13}$$

2.1.4. Calculation of *MOR* and *CMOD*

The beam flexural strength, expressed in terms of a modulus of rupture (MOR), is expected to be reached when the fracture process zone is partially-developed, t, after some stable crack growth stage. For a given initial crack size (a_i), crack extension ($a - a_i$) and a *trial* value of crack-mouth-opening displacement w, the crack is assumed to propagate once the total stress intensity factor K_I is equal to the critical value K_{IC}.

$$K_{IC} = K_{IM}(\sigma_f, d, r) - K_{I\sigma}(T_b, d, u, r_i, r) \tag{14}$$

In which $r_i = a_i/d$, $r = a/d$, and $u = w/w_c$. From the above equation, one can calculate the flexural stress σ_f at which the crack will further propagate with increased loading as follows:

$$\sigma_f = \frac{K_{IC}+K_{I\sigma}(T_b,d,u,r_i,r)}{\sqrt{\pi dr}\,f_3(r)} \tag{15}$$

From the above equation and Eq 13, a refined estimate of crack-mouth-opening displacement w (expressed in the normalized form $u = w/w_c$) can be computed as follows:

$$u = \frac{w_M(\sigma_f,E_c,d,r)-w_\sigma(T_b,E_c,d,u,r_i,r)}{w_c} \tag{16}$$

The above two steps are repeated until converged values of σ_f and u is reached. The crack length, a, is subsequently incremented, and new values of σ_f and u are obtained using the above procedure. This will generate a set of (σ_f, u) values versus normalized crack length, r. These data can be plotted where the peak flexural stress would correspond to the flexural strength (MOR) of the material.

2.2. Experimental program

The experimental program in this study included 13 prism series. In most cases, at least three prism specimens were cast and tested under four-point bending (see Figure 2) to measure the material's flexural strength. The experimental program aimed to evaluate the flexural strength of the SFRC material Based on the effects of fibre volume fraction, fibre type, specimen depth, and concrete compressive strength and compare the observed experimental trends with those predicted by the proposed flexural strength model. A summary of the experimental program is shown in Table 1.

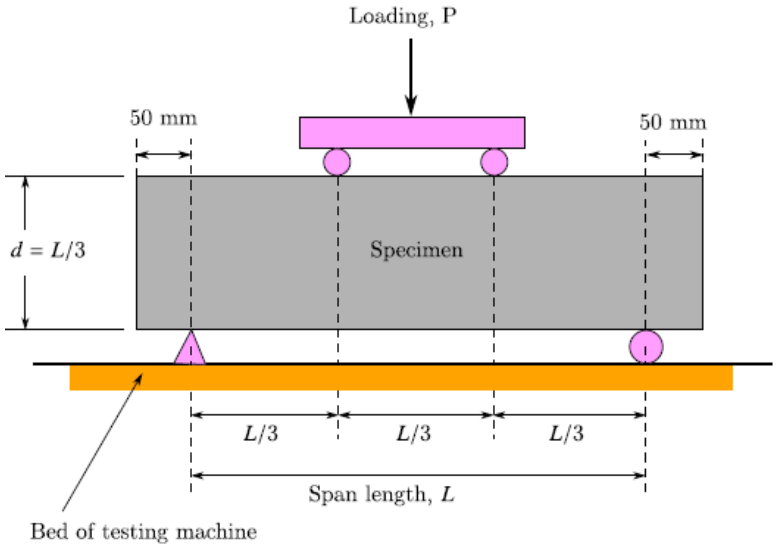

Figure 2. Flexural test setup.

Table 1. Summary of the experimental program.

Specimen ID	Fibre type	Volume fraction V_f (%)	Depth d (mm)	Grade of concrete f_{cu} (MPa)	Average flexural strength (MPa)
100-0-40	-	0	100	40	4.70
100-OL13-1-40	OL13/0.2	1	100	40	5.45
100-OL13-1.5-40	OL13/0.2	1.5	100	40	5.95
100-OL13-2-40	OL13/0.2	2	100	40	7.85
100-RL45-1-40	RL45/40	1	100	40	4.95
100-RL45-1.5-40	RL45/40	1.5	100	40	6.42
100-RL45-2-40	RL45/40	2	100	40	6.01
100-ZP305-1-40	ZP305	1	100	40	5.33
100-ZP305-1-50	ZP305	1	100	50	5.48
100-ZP305-1-60	ZP305	1	100	60	5.70
100-ZP305-1-70	ZP305	1	100	70	6.58
150-ZP305-1-40	ZP305	1	150	40	4.59
200-ZP305-1-40	ZP305	1	200	40	3.50

2.2.1. Materials and test specimens

The raw materials used to prepare the concrete mixes were commercially-available Ordinary Portland Cement, coarse aggregates of 10 mm maximum size, and fine aggregates. Four different concrete mixes corresponding to four different concrete cube compressive strengths (40, 50, 60, and 70 MPa) were included in the experimental program. Two different steel fibres: straight-end (OL13/0) and hooked-end (RL45/40 and ZP305), and three fibre volume fractions: 1%, 1.5%, and 2% were used in the SFRC mixes. Further, three different specimen depths (100 mm, 150 mm, and 200 mm) were considered when casting the SFRC prisms to study the effect of specimen size on the flexural strength of the SFRC. Tables 2 and 3 provide further details about the concrete mix design and the geometrical and mechanical properties of the steel fibres used in the SFRC mixes.

The test samples are labeled and identified through their depth, fibre type, dosage, and compressive strength of the mix to cast the samples. For example, test sample 100-OL-1-40 refers to the specimen with 100 mm depth, 1% fibre volume fraction of type OL13/0.2, and 40 MPa concrete compressive strength. The specimen dimensions and loading test setup followed the ASTM C1609 standard.

Table 2. Fibre geometrical and mechanical properties.

Fibre type	Length L_f (mm)	Diameter d_f (mm)	Aspect ratio L_f/d_f	Modulus of elasticity E_f (GPa)	Fibre tensile strength (MPa)	Fibre density (kg/m^3)
OL13/0.2	13	0.2	65	200	2600	7850
RL45/40	40	0.9	45	200	1100	7850
ZP305	30	0.55	55	200	1100	7850

Table 3. Concrete mix design.

Compressive strength (MPa)	Cement	Coarse aggregate-cement ratio	Fine aggregate-cement ratio	Water-to-cement ratio
40	1	1.74	2.36	0.58
50	1	1.46	1.90	0.485
60	1	1.25	1.53	0.43
70	1	0.925	1.09	0.37

2.2.2. Testing procedure

An Instron testing machine was used to load the prism specimens under a displacement-controlled mode and four-point bending configuration. The loading rate was initially set at a constant rate of 0.1 mm/min and then increased to 0.3 mm/min after reaching the peak load. Both the applied load (P) and midspan deflection were measured during the experiment. From each test, the flexural strength was calculated from the equation: $\sigma_f = 1000\, P_u L/bd^2$, where P_u is the maximum load (in kN) measured for a given prism specimen, and L, b, and d are the clear span, width, and depth of the specimen (all in mm), respectively.

2.2.3. Experimental results

The failure of SFRC prisms happened after forming single or double cracks in the constant moment region, as shown in Figure 3. In some of the samples, initial crack propagation did not start in the midspan region of the prism (i.e., crack initiated within the constant-moment region). Some of the tested prisms exhibited dual crack initiation and propagation. However, in all cases, only one crack propagated further as the load increased until failure. This is in line with the expectation that in SFRC, with a relatively low volume fraction of fibres, a single crack will propagate until the complete failure of the specimen.

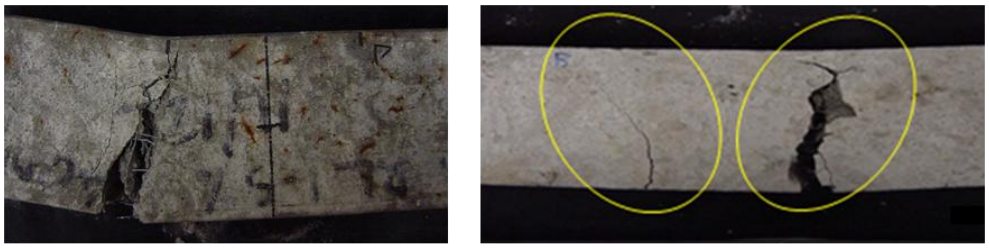

(a) (b)

Figure 3. Observed crack patterns in sample test specimens (a) single-crack failure pattern; (b) double-crack failure pattern.

A summary of the experimental results is presented in Table 1. For most test parameters, at least three identical samples were tested, and the corresponding flexural stress-midspan deflection ($\sigma_f - \Delta$)

curves are plotted in a single graph as shown in Figures 4–7, which also report the average flexural strength (or Modulus Of Rupture, MOR) for the mix. In the following subsections, these results are exploited to discuss the effect of test parameters on flexural strength.

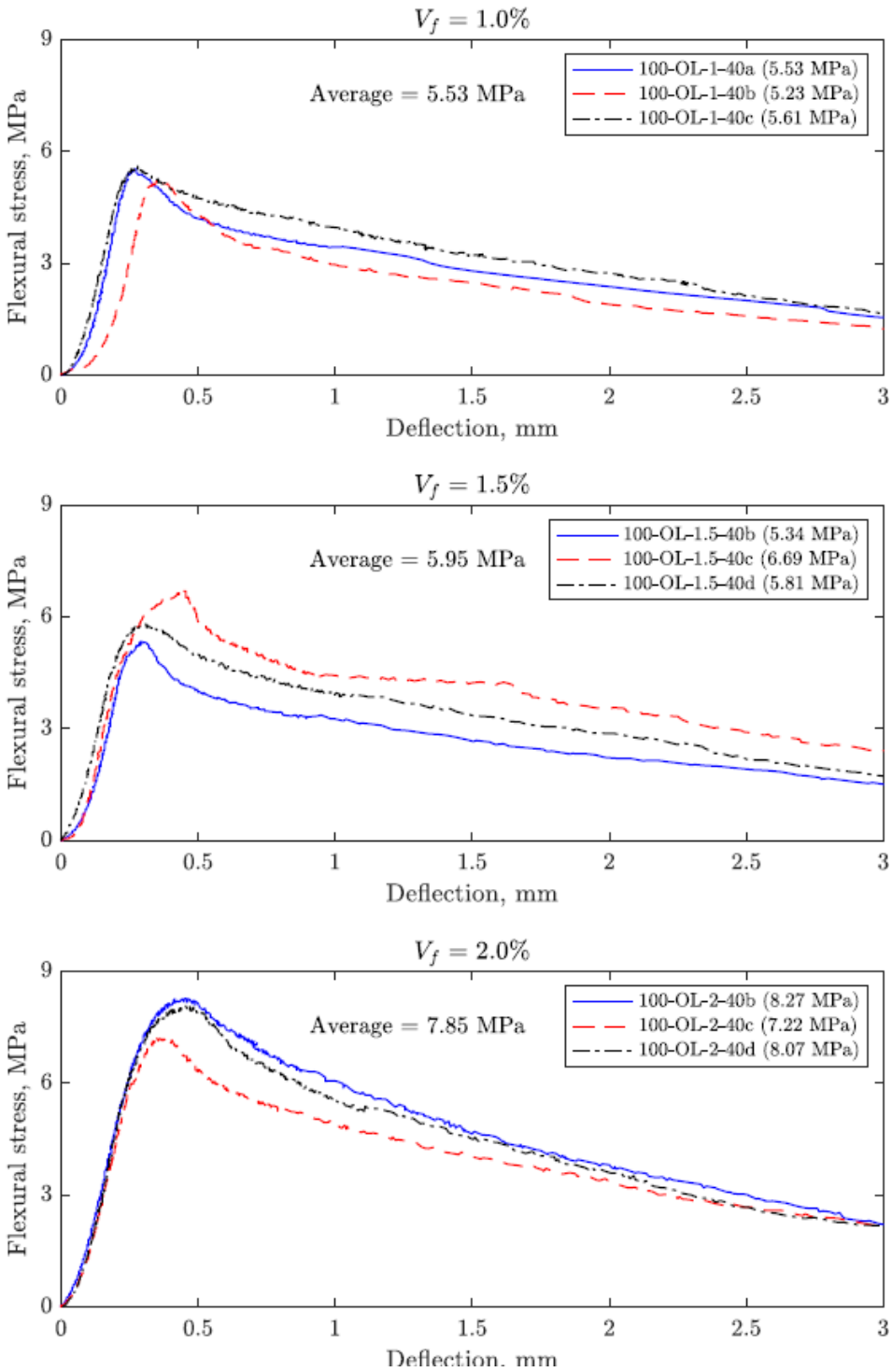

Figure 4. Effect of fibre volume fraction on the flexural stress-deflection response of OL specimen series (d = 100 mm, f_{cu} = 40 MPa).

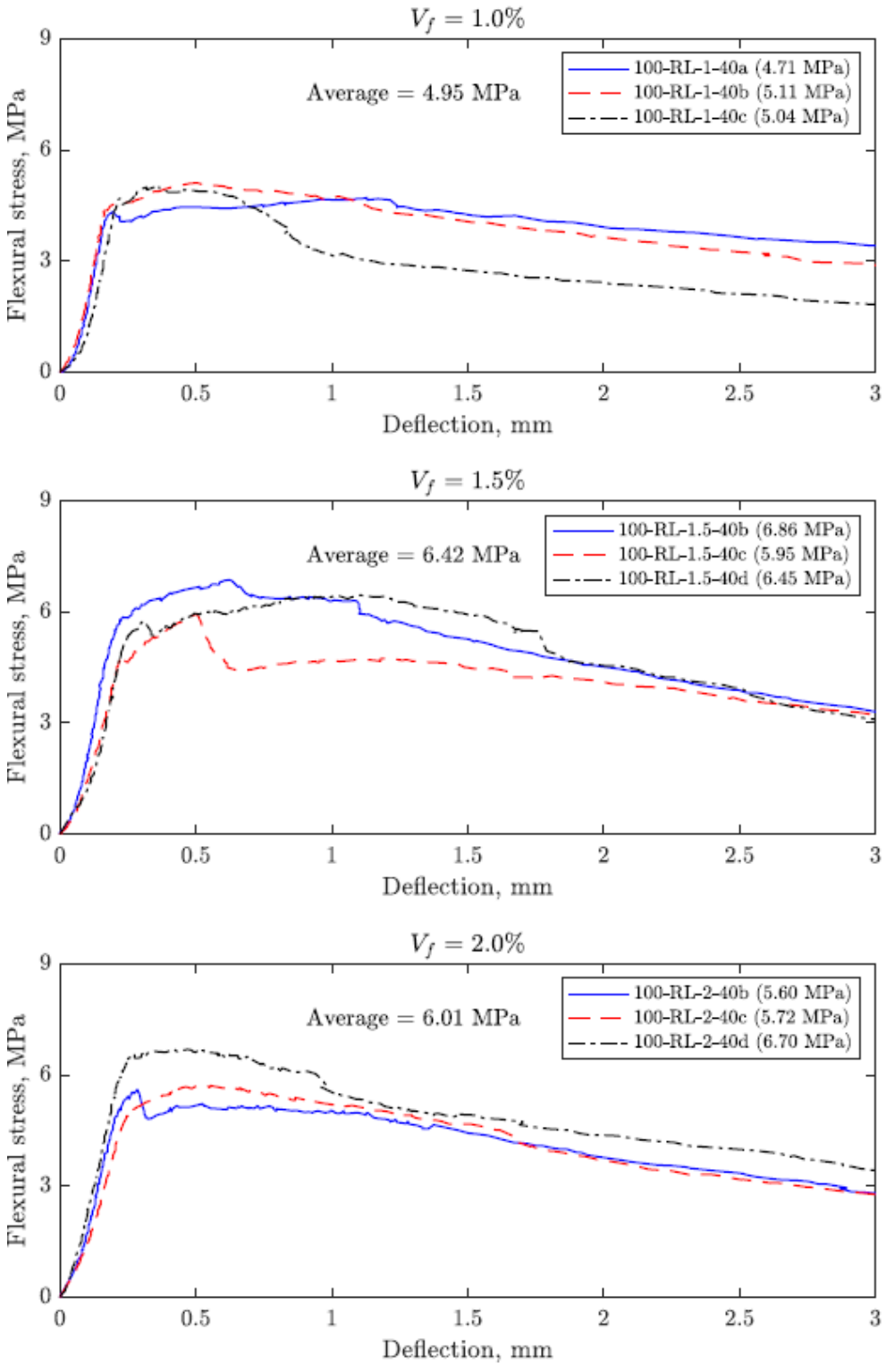

Figure 5. Effect of fibre volume fraction on the flexural stress-deflection response of RL specimen series (d = 100 mm, f_{cu} = 40 MPa).

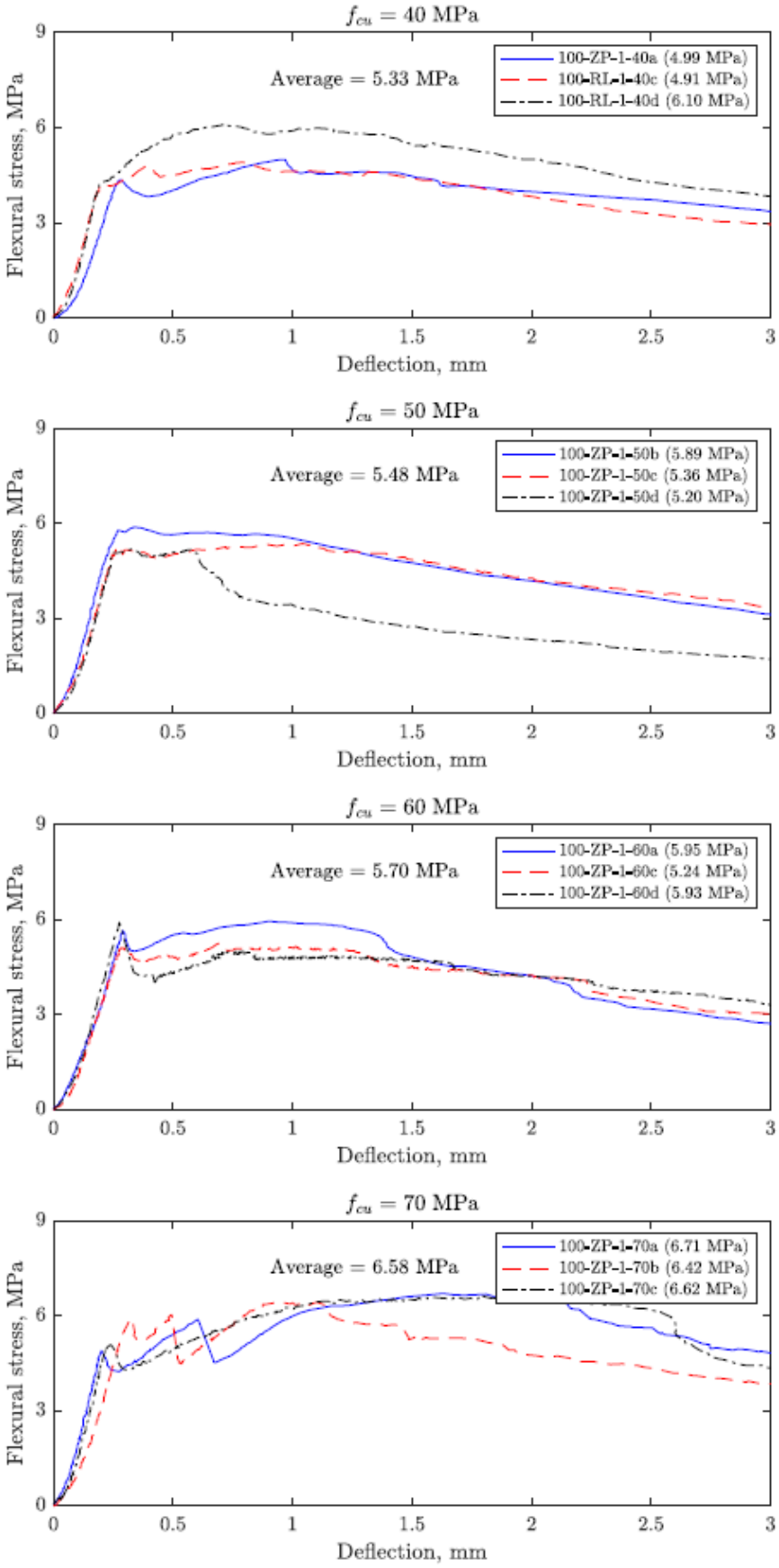

Figure 6. Effect of compressive strength on the flexural stress-deflection response of RL specimen series (d = 100 mm, V_f = 1%).

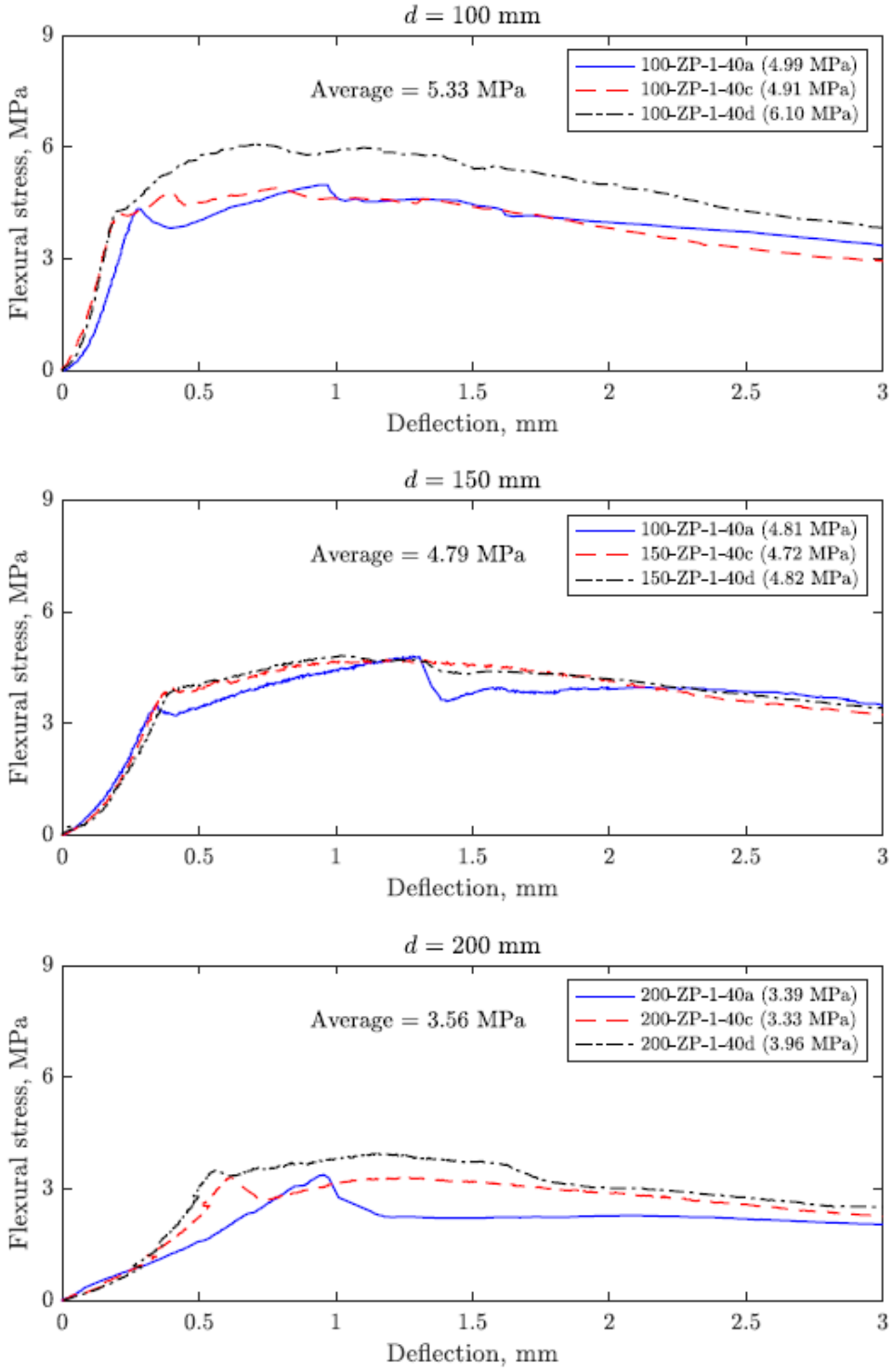

Figure 7. Effect of specimen depth on the flexural stress-deflection response of ZP specimen series (f_{cu} = 40 MPa, V_f = 1%).

(a) Effect of volume fraction of fibres *(V_f)*

OL13/0.2 Fibres (Straight-End): Figure 4 shows the flexural stress-midspan deflection curves for three series of specimens, each consisting of 100 mm duplicate prisms cast with 40 MPa concrete

and incorporating 1%, 1.5%, and 2%. In all series, a single or two significant cracks formed on the tensile face of the prism within the constant moment region and propagated to the compression face with the increase in mid-span deflection. The crack propagation was initially associated with the increase in flexural stress until a peak value was reached, then dropped as the crack continued to propagate, accompanied by the increase in mid-span deflection. The measured flexural strengths (or MOR) for the 1%, 1.5%, and 2% specimen series were 5.45 MPa, 5.95 MPa, and 7.85 MPa, respectively, which correspond to 16%, 27%, and 67% increase in the flexural strength of the material compared to the control specimen.

RL45 Fibres (Hooked-End): Figure 5 shows the flexural stress-midspan deflection curves for the RL specimen series, which incorporated 1%, 1.5%, and 2% hooked-end steel fibres (RL45/40, $L_f = 40$ mm). For these series, the observed crack initiation and propagation and associated flexural stress-deflection responses were similar to those discussed earlier for the OL series. However, for the RL series, the increase in the fibre volume fraction had a lesser impact on the measured flexural strength than the OL series. The measured flexural strengths for the 1%, 1.5%, and 2% specimens were 4.95 MPa, 6.42 MPa, and 6.06 MPa, respectively, corresponding to 5%, 37%, and 28% increase over the control specimen. These results are attributed to the relatively long length of the RL fibres and their end geometry (hooked-end) which resulted in reduced workability of the SFRC fresh mix, especially at 2% fibre volume fraction, and hence, reduced fibre-reinforcing efficiency. On the other hand, the longer length of the RL fibres contributed towards the more effective bridging of the major crack at large crack openings and allowed the specimen to sustain higher flexural stresses with increased mid-span deflections. This resulted in the apparent strain-hardening behaviour shown in Figure 5 for the RL series.

(b) Effect of concrete compressive strength

Figure 6 shows the flexural stress-deflection responses of prism specimens incorporating 1% ZP hooked end fibres and concrete of varying compressive strength (f_{cu} = 40, 50, 60, and 70 MPa). The figure shows that the flexural strength had marginally increased with increased concrete compressive strength from 40 MPa to 60 MPa. However, at 70 MPa compressive strength, the increase in flexural strength (relative to the 40 MPa specimens) was more notable, with an average percentage increase of 28%. Furthermore, these specimens could sustain high flexural stresses for larger deflections compared to their 40–60 MPa concrete counterparts. This indicates that with a sufficient increase in concrete compressive strength (achieved with reduced water-to-cement ratio), the crack propagation and stress transfer mechanism across the main crack due to the bridging action of fibres is enhanced to the extent that it increases the capacity of the specimens to sustain higher flexural stresses under larger deflections. Possible factors responsible for such enhancement include the expected increase in modulus of elasticity and fracture toughness of concrete and a potential increase in the fibre/concrete interfacial bond strength associated with increased concrete compressive strength.

(c) Effect of specimen depth

Figure 7 shows the flexural stress-deflection responses of prism specimens incorporating 1% ZP

hooked-end fibres, 40 MPa concrete, and varying specimen depths (d = 100, 150, and 200 mm). The measured average flexural strength values were 5.33 MPa, 4.79 MPa, and 3.56 MPa for specimens having 100 mm, 150 mm, and 200 mm depth, respectively. Upon comparison, it can be observed that the increase in specimen depth resulted in an apparent reduction of the measured flexural strength. This observed decrease in the measured flexural strength with increased specimen depth is consistent with findings reported in the literature on the size effect observed in fibre-reinforced cement-based composites [33–35].

3. Results and discussions

3.1. Comparison of model predictions to experimental results

This section compares the flexural strength predicted by the proposed model to the test results presented earlier in Section 4. For the model predictions, the following assumptions are made:

- The flexural strength depends on the material tension-softening relationship, expressed in terms of the parameters T_b, w_c, k, and p. These have been computed following the equations provided by Maalej and Li [14], assuming a snubbing friction coefficient f of 0.8 [36] and an interfacial frictional bond strength τ of 3.0 MPa, and 4.0 MPa, for straight-end and hooked-end fibres, respectively.
- The fracture toughness, K_{IC}, was assumed to vary with concrete cube strength according to the equation: $K_{IC} = 0.9 + 0.0075(f_{cu} - 40)$ MPa $\sqrt{\text{m}}^{1/2}$. In calibrating this equation, the authors have referred to fracture toughness data published in references [10,37–39].
- The modulus of elasticity of the concrete was computed following the BS 8110: $E_c = 1000(20 + 0.2f_{cu})$ MPa [40].
- All prisms were assumed to have an initial crack size a_i equal to 10% of the specimen depth.

3.1.1. ffect of fibre volume fraction

The fibre volume fraction within the SFRC is expected to significantly affect the material's flexural strength [41,42]. With a higher percentage of fibres, greater closing stress is expected to act across the crack faces, reducing stress intensity. Therefore, a higher load is required to induce failure. Figures 8 and 9 show a comparison between the model and experimental results for the OL (straight-end) and RL (hooked-end) specimen series, respectively, where the test specimens have a depth of 100 mm, a compressive strength of 40 MPa, and incorporate three different fibre volume fractions (1%, 1.5%, and 2%). Both model predictions and experimental results show increasing flexural strength with increasing fibre volume fraction with a reasonable agreement between the two. The mean error ranges from −22% and 23% for OL specimens and between −24% and 12% for RL specimens. We can also see that in most cases, the model predictions fall within the experimental data range, except for the 2% RL specimen series, where the model overestimated the experimentally-measured flexural strength values. As discussed earlier, the latter is probably due to the tendency for the hooked-end RL fibres to ball (a phenomenon known as balling effect) at this relatively high fibre volume fraction. This effect would lead to uneven distribution of the fibres

within the mix and reduced interfacial bond between the fibres and the matrix, thereby negatively affecting the measured flexural strength.

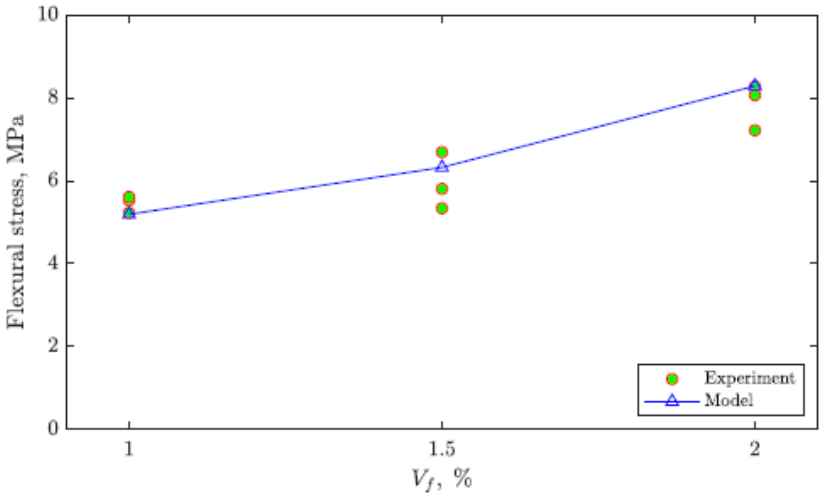

Figure 8. Effect of fibre volume fraction on the flexural strength of OL specimen series (d = 100 mm, f_{cu} = 40 MPa).

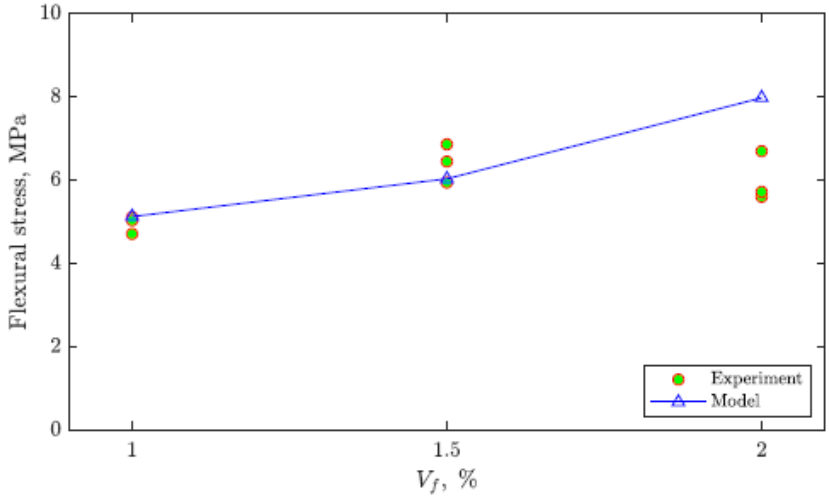

Figure 9. Effect of fibre volume fraction on the flexural strength of RL specimen series (d = 100 mm, f_{cu} = 40 MPa).

3.1.2. Effect of concrete compressive strength

The compressive strength of the concrete has been reported in the literature to affect the flexural strength of SFRC [41–43]. Figure 10 shows a comparison between the model and experimental results for the ZP (hooked-end) specimen series where the specimen depth was equal to 100 mm and the fibre volume fraction was equal to 1% cast using concrete with different compressive strengths (40 MPa, 50 MPa, 60 MPa, and 70 MPa).

The figure shows that the model predictions coincide reasonably well with the experimental results. For instance, the average error ranged from −16% and 6%. The predicted flexural strength for each compressive strength falls within 8% of the measured average value. Consistent with results published in the literature, both model predictions and experimental results indicate that the flexural strength of SFRC increases with the increasing compressive strength of concrete. These results are reasonable considering that the modulus of elasticity of concrete would increase with increased compressive strength, and the crack opening displacement for any given applied moment would decrease. The latter would translate into an increased magnitude of the closing stress acting across the crack faces due to the bridging action of fibres, thereby delaying crack propagation and increasing the load required to reach failure. Further enhancement of the failure load will also result from the assumed increase in fracture toughness and the possible increase in fibre/matrix bond strength due to increased concrete compressive strength. For the present ZP specimen series, the fibre/matrix bond strength was assumed to be constant at 4 MPa.

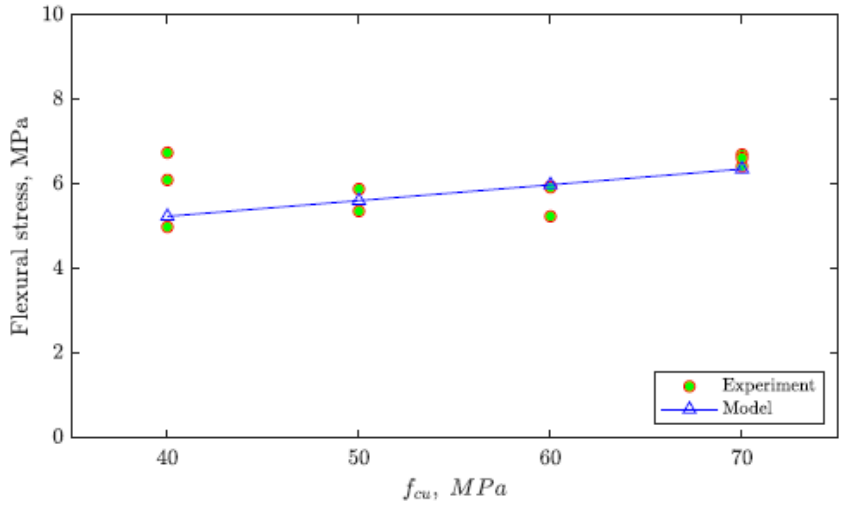

Figure 10. Effect of concrete compressive strength on the flexural strength of ZP specimen series (d =100 mm, V_f = 1%).

3.1.3. Effect of beam depth

The effect of specimen depth on FRC's flexural strength has long been recognized in the literature as the size effect. The flexural strength of FRC tends to decrease with increasing specimen depth. This was because the fracture process zone ahead of the major crack becomes less significant as the depth of the specimen increases. The availability of an analytical model that allows this size effect to be accounted for in design would be useful.

Figure 11 shows a comparison between the model and experimental results for the ZP (hooked-end) specimen series, where the concrete compressive strength was equal to 40 MPa, and the fibre volume fraction was equivalent to 1% with varying specimen depths (100 mm, 150 mm, and 200 mm). The figure indicates that the model predictions and experimental results show decreasing flexural strength with increasing specimen depth. It can be seen that the model predictions fall within the

experimental data range for the 100 mm and 150 mm specimen depths (mean error between −3% and 19%). However, the 200 mm specimen depth model overestimated the average flexural strength by about 55%, with the predicted value deviating from experimental measurements by 16 to 29%. Such deviation may be due to the relatively large size of the specimen, where there is a higher probability for larger defects (beyond the assumed 10% of specimen depth) to be present in the specimen [44], leading to a flexural strength that is lower than predicted by the model.

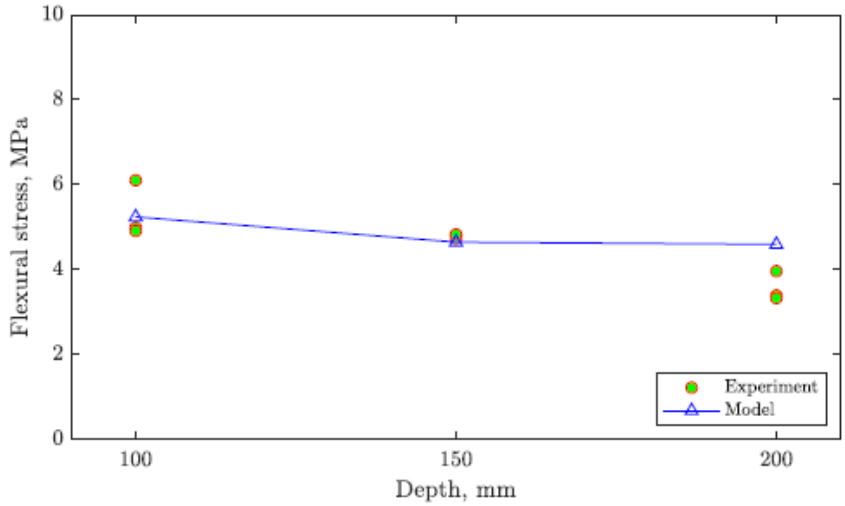

Figure 11. Effect of specimen depth on the flexural strength of ZP specimen series (f_{cu} = 40 MPa, V_f = 1%).

4. Conclusions

This paper presents a fracture mechanics model for predicting the flexural strength of SFRC beams. The model follows the bridged crack model (BCM) approach but assumes a quadratic tension-softening relationship (σ–δ) governing the bridging action of the steel fibres and a linear profile of the propagating crack. For model verification, a companion experimental program was designed to study the variation of the flexural strength of SFRC as a function of fibre type, fibre volume fraction, concrete strength, and specimen depth. The experimental program included 13 specimen series where the SFRC mixes incorporated two types of steel fibres (straight-end and hooked-end), four concrete cube compressive strengths (40, 50, 60, and 70 MPa), three fibre volume fractions (1, 1.5, and 2%), and three specimen depths (100, 150, and 200 mm). The results obtained from the experimental program were compared to those predicted by the proposed flexural strength model. The following is a summary of the main findings.

- A reasonable agreement was observed between the model-predicted and experimentally-measured flexural strength values for all specimen series.
- The model captured the observed variation of the flexural strength of SFRC as a function of the various test parameters, including the fibre volume fraction, the concrete compressive strength, and the specimen depth.

- The model provided useful physical explanations for the observed variation of the flexural strength of SFRC.
- Knowing basic material properties, such as concrete compressive strength, fracture toughness, fibre and fibre/matrix interface properties, specimen geometry, and initial flaw size, would be possible to predict and optimize the flexural strength of a given SFRC material for a given structural application.

Acknowledgments

Partial support for this research by the Sustainable Construction Materials and Structural Systems (SCMASS) Research Group, Institute of Research for Sciences and Engineering (RISE), University of Sharjah, is gratefully acknowledged and appreciated.

Conflict of Interest

The authors declare that the research was conducted without any commercial or financial relationships that could be construed as a potential conflict of interest.

References

1. Li VC, Maalej M (1996) Toughening in cement based composites. Part I: concrete, mortar, and concrete. *Cement Concrete Comp* 18: 223–237. https://doi.org/10.1016/0958-9465(95)00028-3
2. Li VC, Maalej M (1996) Toughening in cement based composites. Part II: Fiber reinforced cementitious composites. *Cement Concrete Comp* 18: 239–249. https://doi.org/10.1016/0958-9465(95)00029-1
3. Hillerborg A, Modéer M, Petersson PE (1976) Analysis of crack formation and crack growth In concrete by means of fracture mechanics and finite elements. *Cement Concrete Res* 6: 773–781. https://doi.org/10.1016/0008-8846(76)90007-7
4. Hillerborg A (1978) A model for fracture analysis. TVBM-3005. Available from: https://portal.research.lu.se/en/publications/a-model-for-fracture-analysis.
5. Bažant ZP (1992) Should design codes consider fracture mechanics size effect?, In: Gerstle W, Bazant ZP, *Concrete Design Based on Fracture Mechanics*, American Concrete Institute, 134: 1–24.
6. Carpinteri A (1981) A fracture mechanics model for reinforced concrete collapse. Available from: https://www.e-periodica.ch/cntmng?pid=bse-re-001:1981:34::9.
7. Carpinteri A (1984) Stability of fracturing process in RC beams. *J Struct Eng* 110: 544–558. https://doi.org/10.1061/(ASCE)0733-9445(1984)110:3(544)
8. Bazant ZP, Pfeiffer A (1987) Determination of fracture energy from size effect and brittleness number. *ACI Mater J* 84: 463–480. https://doi.org/10.14359/2526
9. Bažant ZP, Oh BH (1983) Crack band theory for fracture of concrete. *Mat Constr* 16: 155–177. https://doi.org/10.1007/BF02486267

10. Jenq Y, Shah SP (1985) Two parameter fracture model for concrete. *J Eng Mech* 111: 1227–1241. https://doi.org/10.1061/(ASCE)0733-9399(1985)111:10(1227)
11. Xu S, Reinhardt HW (2000) A simplified method for determining double-K fracture parameters for three-point bending tests. *Int J Fract* 104: 181–209. https://doi.org/10.1023/A:1007676716549
12. Xu S, Reinhardt HW (1999) Determination of double-K criterion for crack propagation in quasi-brittle fracture, Part I : Experimental investigation of crack propagation. *Int J Frac* 98: 111–149. https://doi.org/10.1023/A:1018668929989
13. Xu S, Reinhardt HW (1999) Determination of double-K criterion for crack propagation in quasi-brittle fracture, Part II : Analytical evaluating and practical measuring methods for three-point bending notched beams. *Int J Fract* 98: 151–177. https://doi.org/10.1023/A:1018740728458
14. Maalej M, Li VC (1995) Flexural strength of fiber cementitious composites. J Materi Civil Eng 6: 390–406. https://doi.org/10.1061/(ASCE)0899-1561(1994)6:3(390)
15. Maalej M, Li VC, Hashida T (1995) Effect of fiber rupture on tensile properties of short fiber composites. *J Eng Mech (ASCE)* 121: 903. https://doi.org/10.1061/(ASCE)0733-9399(1995)121:8(903)
16. Zhang J, Li VC (2004) Simulation of crack propagation in fiber-reinforced concrete by fracture mechanics. *Cem Concr Res* 34: 333–339. https://doi.org/10.1016/j.cemconres.2003.08.015
17. Accornero F, Rubino A, Carpinteri A (2020) Ductile-to-brittle transition in fiber-reinforced concrete beams: Scale and fiber volume fraction effects. *MDPC* 2020: 1–11. https://doi.org/10.1002/mdp2.127
18. Accornero F, Rubino A, Carpinteri A (2022) A fracture mechanics approach to the design of hybrid-reinforced concrete beams. *Eng Fract Mech* 275: 108821. https://doi.org/10.1016/j.engfracmech.2022.108821
19. Carpinteri A, Accornero F, Rubino A (2022) Scale effects in the post-cracking behaviour of fibre-reinforced concrete beams. *Int J Fract*. https://doi.org/10.1007/s10704-022-00671-x
20. Accornero F, Rubino A, Carpinteri A (2022) Post-cracking regimes in the flexural behaviour of fibre-reinforced concrete beams. *Int J Solids Struct* 248: 111637. https://doi.org/10.1016/j.ijsolstr.2022.111637
21. Accornero F, Rubino A, Carpinteri A (2022) Ultra-low cycle fatigue (ULCF) in fibre-reinforced concrete beams. *Theor Appl Fract Mec* 120: 103392. https://doi.org/10.1016/j.tafmec.2022.103392
22. Lok TS, Xiao JR (1999) Flexrual strength assessment of fiber reinforced concrete. *J Mater Civil Eng* 11: 118–196. https://doi.org/10.1061/(ASCE)0899-1561(1999)11:3(188)
23. Meng G, Wu B, Xu S, et al. (2021) Modelling and experimental validation of flexural tensile properties of steel fiber reinforced concrete. *Constr Build Mater* 273: 121974. https://doi.org/10.1016/j.conbuildmat.2020.121974
24. Zeng JJ, Zeng WB, Ye YY, et al. (2022) Flexural behavior of FRP grid reinforced ultra-high-performance concrete composite plates with different types of fibers. *Eng Struct* 272: 115020. https://doi.org/10.1016/j.engstruct.2022.115020

25. Soetens T, Matthys S (2014) Different methods to model the post-cracking behaviour of hooked-end steel fibre reinforced concrete. *Constr Build Mater* 73: 458–471. https://doi.org/10.1016/j.conbuildmat.2014.09.093
26. Zhang J, Leung CK, Xu S (2010) Evaluation of fracture parameters of concrete from bending test using inverse analysis approach. *Mater Struct* 43: 857–874. https://doi.org/10.1617/s11527-009-9552-5
27. Da Silva CN, Ciambella J, Barros JAO, et al. (2020) A multiscale model for optimising the flexural capacity of FRC structural elements. *Compos Part B-Eng* 200: 108325. https://doi.org/10.1016/j.compositesb.2020.108325
28. Bhosale AB, Prakash SS (2020) Crack propagation analysis of synthetic vs. steel vs. hybrid fibre-reinforced concrete beams using digital image correlation technique. *Int J Concr Struct M* 14: 1–19. https://doi.org/10.1186/s40069-020-00427-8
29. Kravchuk R, Landis EN (2018) Acoustic emission-based classification of energy dissipation mechanisms during fracture of fiber-reinforced ultra-high-performance concrete. Constr Build Mater 176: 531–538. https://doi.org/10.1016/j.conbuildmat.2018.05.039
30. Chen C, Chen X, Ning Y (2022) Identification of fracture damage characteristics in ultra-high performance cement-based composite using digital image correlation and acoustic emission techniques. *Compos Struct* 291: 115612. https://doi.org/10.1016/j.compstruct.2022.115612
31. He F, Biolzi L, Carvelli V, et al. (2022) Digital imaging monitoring of fracture processes in hybrid steel fiber reinforced concrete. *Compos Struct* 298: 116005. https://doi.org/10.1016/j.compstruct.2022.116005
32. Tada H, Paris PC, Irwin GR (2000) *The Stress Analysis of Crack Handbook*, 3 Eds., ASME Press. https://doi.org/10.1115/1.801535
33. Ward RJ, Li VC (1991) Dependence of flexural behaviour of fibre reinforced mortar on material fracture resistance and beam size. *Constr Build Mater* 5: 151–161. https://doi.org/10.1016/0950-0618(91)90066-T
34. Johnston CD (1982) Steel fiber reinforced and plain concrete: factors influencing flexural strength measurement. *ACI J Proc* 79: 131–138. https://doi.org/10.14359/10888
35. Yoo DY, Banthia N, Yang JM, et al. (2016) Size effect in normal- and high-strength amorphous metallic and steel fiber reinforced concrete beams. *Constr Build Mater* 121: 676–685. https://doi.org/10.1016/j.conbuildmat.2016.06.040
36. Li VC, Wang Y, Backer S (1900) Effect of inclining angle, bundling and surface treatment on synthetic fibre pull-out from a cement matrix. *Composites* 21: 132–140. https://doi.org/10.1016/0010-4361(90)90005-H
37. Ince R (2012) Determination of concrete fracture parameters based on peak-load method with diagonal split-tension cubes. *Eng Fract Mech* 82: 100–114. https://doi.org/10.1016/j.engfracmech.2011.11.026
38. Chbani H, Saadouki B, Boudlal M, et al. (2019) Determination of fracture toughness in plain concrete specimens by R curve. *Frat Integrita Strut* 13: 763–774. https://doi.org/10.3221/IGF-ESIS.49.68

39. Xu S, Zhang X (2008) Determination of fracture parameters for crack propagation in concrete using an energy approach. *Eng Fract Mech* 75: 4292–4308. https://doi.org/10.1016/j.engfracmech.2008.04.022
40. British Standards Institution (2007) Structural use of concrete-part 1 : code of practice for design and construction. Available from: https://crcrecruits.files.wordpress.com/2014/04/bs8110-1-1997-structural-use-of-concrete-design-construction.pdf
41. Lee J, Cho B, Choi E (2017) Flexural capacity of fiber reinforced concrete with a consideration of concrete strength and fiber content. *Constr Build Mater* 138: 222–231. https://doi.org/10.1016/j.conbuildmat.2017.01.096
42. Yoo DY, Yoon YS, Banthia N (2015) Flexural response of steel-fiber-reinforced concrete beams: Effects of strength, fiber content, and strain-rate. *Cement Concrete Compos* 64: 84–92. https://doi.org/10.1016/j.cemconcomp.2015.10.001
43. Jang SJ, Jeong GY, Lee MH, et al. (2016) Compressive strength effects on flexural behavior of steel fiber reinforced concrete. *Key Eng Mater* 709: 101–104. https://doi.org/10.4028/www.scientific.net/KEM.709.101
44. Soutsos M, Domone P (2017) *Construction Materials: Their Nature and Behaviour*, CRC Press. https://doi.org/10.1201/9781315164595